

# The drive system of the Major Atmospheric Gamma-ray Imaging Cherenkov Telescope

T. Bretz<sup>a,\*</sup>, D. Dorner<sup>a</sup>, R. M. Wagner<sup>b</sup>, P. Sawallisch<sup>b</sup>

<sup>a</sup>Universität Würzburg, Am Hubland, 97074 Würzburg, Germany

<sup>b</sup>Max-Planck-Institut für Physik, Föhringer Ring 6, 80805 München, Germany

---

## Abstract

The MAGIC telescope is an imaging atmospheric Cherenkov telescope, designed to observe very high energy gamma-rays while achieving a low energy threshold. One of the key science goals is fast follow-up of the enigmatic and short lived gamma-ray bursts. The drive system for the telescope has to meet two basic demands: (1) During normal observations, the 72-ton telescope has to be positioned accurately, and has to track a given sky position with high precision at a typical rotational speed in the order of one revolution per day. (2) For successfully observing GRB prompt emission and afterglows, it has to be powerful enough to position to an arbitrary point on the sky within a few ten seconds and commence normal tracking immediately thereafter. To meet these requirements, the implementation and realization of the drive system relies strongly on standard industry components to ensure robustness and reliability. In this paper, we describe the mechanical setup, the drive control and the calibration of the pointing, as well as present measurements of the accuracy of the system. We show that the drive system is mechanically able to operate the motors with an accuracy even better than the feedback values from the axes. In the context of future projects, envisaging telescope arrays comprising about 100 individual instruments, the robustness and scalability of the concept is emphasized.

*Key words:* MAGIC, drive system, IACT, scalability, calibration, fast positioning

---

## 1. Introduction

The MAGIC telescope on the Canary Island of La Palma, located 2200 m above sea level at 28°45' N and 17°54' W, is an imaging atmospheric Cherenkov telescope designed to achieve a low energy threshold, fast positioning, and high tracking accuracy [1, 2]. The MAGIC design, and the currently ongoing construction of a second telescope (MAGIC II; [3]), pave the way for ground-based detection of gamma-ray sources at cosmological distances down to less than 25 GeV [4]. After the discovery of the distant blazars 1ES 1218+304 at a redshift of  $z=0.182$  [5] and 1ES 1011+496 at  $z=0.212$  [6], the most recent breakthrough has been the discovery of the first quasar at very high energies, the flat-spectrum radio source 3C 279 at a redshift of  $z=0.536$  [7].

These observational results were somewhat surprising, since the extragalactic background radiation in the mid-infrared to near-infrared wavelength range was believed to be strong enough to inhibit propagation of gamma-rays across cosmological distances [8, 9, 10]. The apparent low level of pair attenuation of gamma-rays greatly improves the prospects of searching for very high energy gamma-rays from gamma-ray bursts (GRBs), cf. [11]. Their remarkable similarities with blazar flares, albeit at much shorter timescales, presumably arise from the scaling behavior of relativistic jets, the common physical cause of these phenomena. Since most GRBs reside at large redshifts, their detection at very high energies relies on the low level of absorption [12]. Moreover, the cosmological absorption decreases with photon energy, favoring MAGIC to discover GRBs due to its low energy threshold.

---

\*Corresponding author: tbretz@astro.uni-wuerzburg.de

Due to the short life times of GRBs and the limited field of view of imaging atmospheric Cherenkov telescopes, the drive system of the MAGIC telescope has to meet two basic demands: during normal observations, the 72-ton telescope has to be positioned accurately, and has to track a given sky position, i.e., counteract the apparent rotation of the celestial sphere, with high precision at a typical rotational speed in the order of one revolution per day. For catching the GRB prompt emission and afterglows, it has to be powerful enough to position the telescope to an arbitrary point on the sky within a very short time and commence normal tracking immediately thereafter. To keep the system simple, i.e., robust, both requirements should be achieved without an indexing gear. The telescope's total weight of 72 tons is comparatively low, reflecting the use of low-weight materials whenever possible. For example, the mount consists of a space frame of carbon-fiber reinforced plastic tubes, and the mirrors are made of polished aluminum.

In this paper, we describe the basic properties of the MAGIC drive system. In section 3, the hardware components and mechanical setup of the drive system are outlined. The control loops and performance goals are described in section 4, while the implementation of the positioning and tracking algorithms and the calibration of the drive system are explained in section 5. The system can be scaled to meet the demands of other telescope designs as shown in section 6. Finally, in section 7 and section 8 we draw conclusions from our experience of operating the MAGIC telescope with this drive system for four years.

## 2. General design considerations

The drive system of the MAGIC telescope is quite similar to that of large, alt-azimuth-mounted optical telescopes. Nevertheless there are quite a few aspects that influenced the design of the MAGIC drive system in comparison to optical telescopes and small-diameter Imaging Atmospheric Cherenkov telescopes (IACT).

Although IACTs have optical components, the tracking and stability requirements for IACTs are much less demanding than for optical telescopes.

Like optical telescopes, IACTs track celestial objects, but observe quite different phenomena: Optical telescopes observe visible light, which originates at infinity and is parallel. Consequently, the best-possible optical resolution is required and in turn, equal tracking precision due to comparably long integration times, i.e., seconds to hours. In contrast, IACTs record the Cherenkov light produced by an electromagnetic air-shower in the atmosphere, induced by a primary gamma-ray, i.e., from a close by (5 km - 20 km) and extended event with a diffuse transverse extension and a typical extension of a few hundred meters. Due to the stochastic nature of the shower development, the detected light will have an inherent limitation in explanatory power, improving normally with the energy, i.e., shower-particle multiplicity. As the Cherenkov light is emitted under a small angle off the particle tracks, these photons do not even point directly to the source like in optical astronomy. Nevertheless, the shower points towards the direction of the incoming gamma-ray and thus towards its source on the sky. For this reason its origin can be reconstructed analyzing its image. Modern IACTs achieve an energy-dependent pointing resolution for individual showers of  $6' - 0.6'$ . These are the predictions from Monte Carlo simulations assuming, amongst other things, ideal tracking. This sets the limits achievable in practical cases. Consequently, the required tracking precision must be at least of the same order or even better. Although the short integration times, on the order of a few nanoseconds, would allow for an offline correction, this should be avoided since it may give rise to an additional systematic error.

To meet one of the main physics goals, the observation of prompt and afterglow emission of GRBs, positioning of the telescope to their assumed sky position is required in a time as short as possible. Alerts, provided by satellites, arrive at the MAGIC site typically within 10s after the outburst [13]. Since the life times of GRBs show a bimodal distribution [14] with a peak between 10s and 100s. To achieve a positioning time to any position on the sky within a reasonable time inside this window, i.e. less than a minute, a very light-weight but sturdy telescope and a fast-acting and powerful drive system is required.

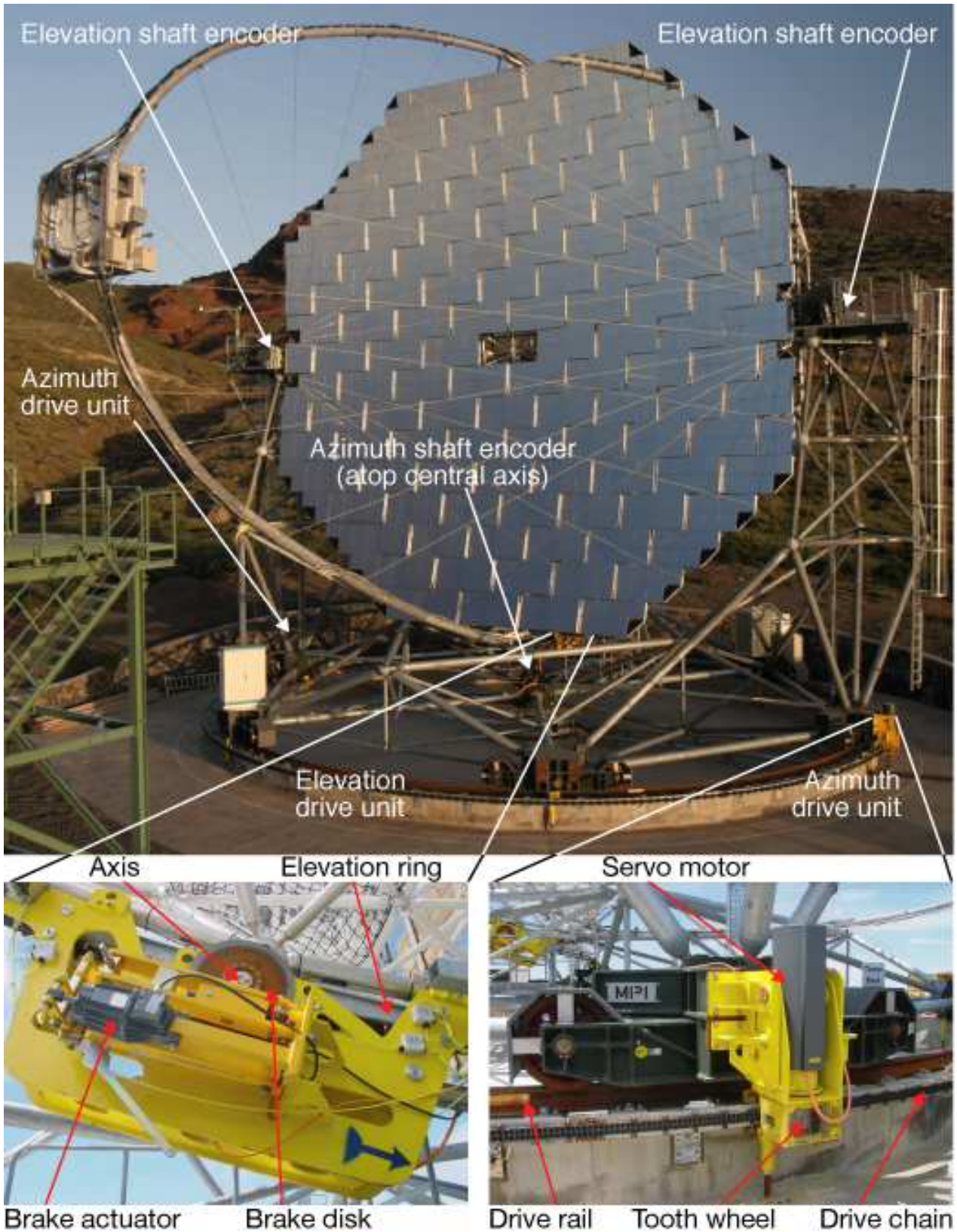


Figure 1: The top picture shows the MAGICI telescope with the major components of the drive system. The elevation drive unit, from its back side, is enlarged in the bottom left picture. Visible is the actuator of the safety holding brake and its corresponding brake disk mounted on the motor-driven axis. The motor is attached on the opposite side. The picture on the bottom right shows one of the azimuth bogeys with its two railway rails. The motor is housed in the grey box on the yellow drive unit. It drives the tooth double-toothed wheel gearing into the chain through a gear and a clutch.

### 3. Mechanical setup and hardware components

The implementation of the drive system relies strongly on standard industry components to ensure robustness, reliability and proper technical support. Its major drive components, described hereafter, are shown on the pictures in fig. 2.

The azimuth drive ring of 20 m diameter is made from a normal railway rail, which was delivered in pre-bent sections and welded on site. Its head is only about 74 mm broad and has a bent profile. The fixing onto the concrete foundation uses standard rail-fixing elements, and allows for movements caused by temperature changes. The maximum allowable deviation from the horizontal plane as well as deviation from flatness is  $\pm 2$  mm, and from the ideal circle it is  $\Delta r = 8$  mm. The rail support was leveled with a theodolite every 60 cm with an overall tolerance of  $\pm 1.5$  mm every 60 cm. In between the deviation is negligible. Each of the six bogeys holds two standard crane wheels of 60 cm diameter with a rather broad wheel tread of 110 mm. This allows for deviations in the 11.5 m-distance to the central axis due to extreme temperature changes, which can even be asymmetric in case of different exposure to sunlight on either side. For the central bearing of the azimuth axis, a high-quality ball bearing was installed fairly assuming that the axis is vertically stable. For the elevation axis, due to lower weight, a less expensive sliding bearing with a teflon layer was used. These sliding bearings have a slightly spherical surface to allow for small misalignments during installation and some bending of the elevation axis stubs under load.

The drive mechanism is based on duplex roller chains and sprocket wheels in a rack-and-pinion mounting. The chains have a breaking strength of 19 tons and a chain-link spacing of 2.5 cm. The initial play between the chain links and the sprocket-wheel teeth is about 3 mm - 5 mm, according to the data sheet, corresponding to much less than an arc-second on the telescope axes. The azimuth drive chain is fixed on a dedicated ring on the concrete foundation, but has quite some radial distance variation of up to 5 mm. The elevation drive chain is mounted on a slightly oval ring below the mirror dish, because the ring forms an integral part of the camera support mast structure.

Commercial synchronous motors (type designation Bosch Rexroth<sup>1</sup> MHD 112C-058) are used together with low-play planetary gears (type designation alpha<sup>2</sup> GTS 210-M02-020 B09, ratio 20) linked to the sprocket wheels. These motors intrinsically allow for a positional accuracy better than one arc-second of the motor axis. Having a nominal power of 11 kW, they can be overpowered by up to a factor five for a few seconds. It should be mentioned that due to the installation height of more than 2200 m a.s.l., due to lower air pressure and consequently less efficient cooling, the nominal values given must be reduced by about 20%. Deceleration is done operating the motors as generator which is as powerful as acceleration. The motors contain 70 Nm holding brakes which are not meant to be used as driving brake. The azimuth motors are mounted on small lever arms. In order to follow the small irregularities of the azimuthal drive chain, the units are forced to follow the drive chain, horizontally and vertically, by guide rolls. The elevation-drive motor is mounted on a nearly 1 m long lever arm to be able to compensate the oval shape of the chain and the fact that the center of the circle defined by the drive chain is shifted 356 mm away from the axis towards the camera. The elevation drive is also equipped with an additional brake, operated only as holding brake, for safety reasons in case of extremely strong wind pressure. No further brake are installed on the telescope.

The design of the drive system control, c.f. Bretz et al. [15], is based on digitally controlled industrial drive units, one for each motor. The two motors driving the azimuth axis are coupled to have a more homogeneous load transmission from the motors to the structure compared to a single (more powerful) motor. The modular design allows to increase the number of coupled devices dynamically if necessary, c.f. Bretz et al. [16].

At the latitude of La Palma, the azimuth track of stars can exceed  $180^\circ$  in one night. To allow for continuous observation of a given source at night without reaching one of the end positions in azimuth. the

---

<sup>1</sup><http://www.boschrexroth.de>  
Bosch Rexroth AG, 97816 Lohr am Main, Germany

<sup>2</sup><http://www.wittenstein-alpha.de>  
Wittenstein alpha GmbH, 97999 Igersheim, Germany

allowed range for movements in azimuth spans from  $\varphi = -90^\circ$  to  $\varphi = +318^\circ$ , where  $\varphi = 0^\circ$  corresponds to geographical North, and  $\varphi = 90^\circ$  to geographical East. To keep slewing distances as short as possible (particularly in case of GRB alerts), the range for elevational movements spans from  $\theta = +100^\circ$  to  $\theta = -70^\circ$  where the change of sign implies a movement *across the zenith*. This so-called *reverse mode* is currently not in use, as it might result in hysteresis effects of the active mirror control system, still under investigation, due to shifting of weight at zenith. The accessible range in both directions and on both axes is limited by software to the mechanically accessible range. For additional safety, hardware end switches are installed directly connected to the drive controller units, initiating a fast, controlled deceleration of the system when activated. To achieve an azimuthal movement range exceeding  $360^\circ$ , one of the two azimuth end-switches needs to be deactivated at any time. Therefore, an additional *direction switch* is located at  $\varphi = 164^\circ$ , short-circuiting the end switch currently out of range.

#### 4. Setup of the motion control system

The motion control system similarly uses standard industry components. The drive is controlled by the feedback of encoders measuring the angular positions of the motors and the telescope axes. The encoders on the motor axes provide information to micro controllers dedicated for motion control, initiating and monitoring every movement. Professional built-in servo loops take over the suppression of oscillations. The correct pointing position of the system is ensured by a computer program evaluating the feedback from the telescope axes and initiating the motion executed by the micro controllers. Additionally, the motor-axis encoders are also evaluated to increase accuracy. The details of this system, as shown in figure 2, are discussed below.

##### 4.1. Position feedback system

The angular telescope positions are measured by three shaft-encoders (type designation Hengstler<sup>3</sup>

<sup>3</sup><http://www.hengstler.de>  
Hengstler GmbH, 78554 Aldingen, Germany

AC61/1214EQ.72OLZ). These absolute multi-turn encoders have a resolution of 4 096 (10 bit) revolutions and 16 384 (14 bit) steps per revolution, corresponding to an intrinsic angular resolution of 1.3' per step. One shaft encoder is located on the azimuth axis, while two more encoders are fixed on either side of the elevation axis, increasing the resolution and allowing for measurements of the twisting of the dish (fig. 3). All shaft encoders used are watertight (IP 67) to withstand the extreme weather conditions occasionally encountered at the telescope site. The motor positions are read out at a frequency of 1 kHz from 10 bit relative rotary encoders fixed on the motor axes. Due to the gear ratio of more than one thousand between motor and load, the 14 bit resolution of the shaft encoder system on the axes can be interpolated further using the position readout of the motors. For communication with the axis encoders, a CAN-bus interface with the CANopen protocol is in use (operated at 125 kbps). The motor encoders are directly connected by an analog interface.

##### 4.2. Motor control

The three servo motors are connected to individual motion controller units (*DKC*, type designation Bosch Rexroth, DKC ECODRIVE 03.3-200-7-FW), serving as intelligent frequency converters. An input value, given either analog or digital, is converted to a predefined output, e.g., command position, velocity or torque. All command values are processed through a chain of built-in controllers, cf. fig. 4, resulting in a final command current applied to the motor. This internal chain of control loops, maintaining the movement of the motors at a frequency of 1 kHz, fed back by the rotary encoders on the corresponding motor axes. Several safety limits ensure damage-free operation of the system even under unexpected operation conditions. These safety limits are, e.g., software end switches, torque limits, current limits or control-deviation limits.

To synchronize the two azimuth motors, a master-slave setup is used. While the master is addressed by a command velocity, the slave is driven by the command torque output of the master. This operation mode ensures that both motors can apply their combined force to the telescope structure without oscillations. In principle it is possible to use a bias torque

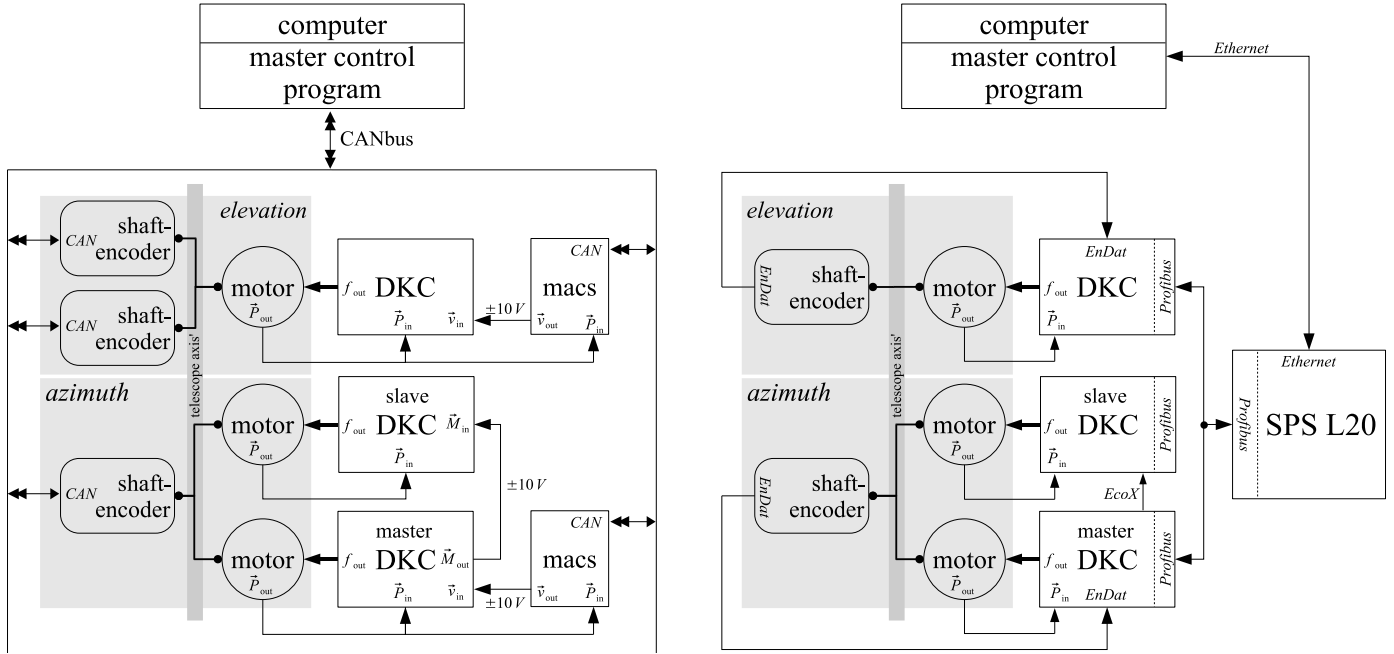


Figure 2: Schematics of the MAGIC I (*left*) and MAGIC II (*right*) drive system. The sketches shows the motors, the motor-encoder feedback as well as the shaft-encoder feedback, and the motion-control units, which are themselves controlled by a superior control, receiving commands from the control PC, which closes the position-control loop. The system is described in more details in section 4.

to eliminate play. This feature was not used because the play is negligible anyhow.

#### 4.3. Motion control

The master for each axis is controlled by presetting a rotational speed defined by  $\pm 10\text{ V}$  on its analog input. The input voltage is produced by a programmable micro controller dedicated to analog motion control, produced by Z&B<sup>4</sup> (MACS, type designation MACS). The feedback is realized through a 500-step emulation of the motor's rotary encoders by the DKCs. Elevation and azimuth movement is regulated by individual MACSs. The MACS controller itself communicates with the control software (see below) through a CANbus connection.

It turned out that in particular the azimuth motor system seems to be limited by the large moment of inertia of the telescope ( $J_{az} \approx 4400\text{ tm}^2$ , for comparison  $J_{el} \approx 850\text{ tm}^2$ ; note that the exact numbers depend on the current orientation of the telescope). At the same time, the requirements on the elevation

drive are much less demanding.

*MAGIC II* For the drive system several improvements have been provided:

- 13 bit absolute shaft-encoders (type designation Heidenhain<sup>5</sup> ROQ 425) are installed, providing an additional sine-shaped  $\pm 1\text{ Vss}$  output within each step. This allows for a more accurate interpolation and hence a better resolution than a simple 14 bit shaft-encoder. These shaft-encoders are also water tight (IP 64), and they are read out via an EnDat 2.2 interface.
- All encoders are directly connected to the DKCs, providing additional feedback from the telescope axes itself. The DKC can control the load axis additionally to the motor axis providing a more accurate positioning, faster movement by improved oscillation suppression and a better motion control of the system.

<sup>4</sup><http://www.zub.de>  
zub machine control AG, 6074 Kastanienbaum, Switzerland

<sup>5</sup><http://www.heidenhain.de>  
Dr. Johannes Heidenhain GmbH, 83301 Traunreut, Germany

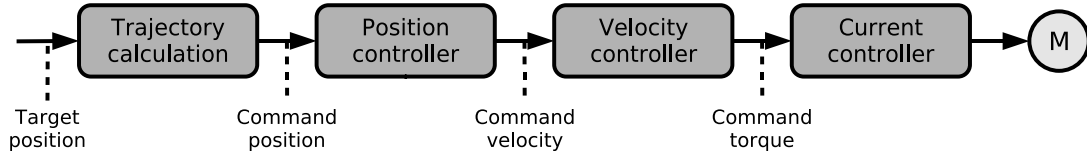


Figure 4: The internal flow control between the individual controllers inside the drive control unit. Depending on the type of the command value, different controllers are active. The control loops are closed by the feedback of the rotary encoder on the motor, and a possible controller on the load axis, as well as the measurement of the current.

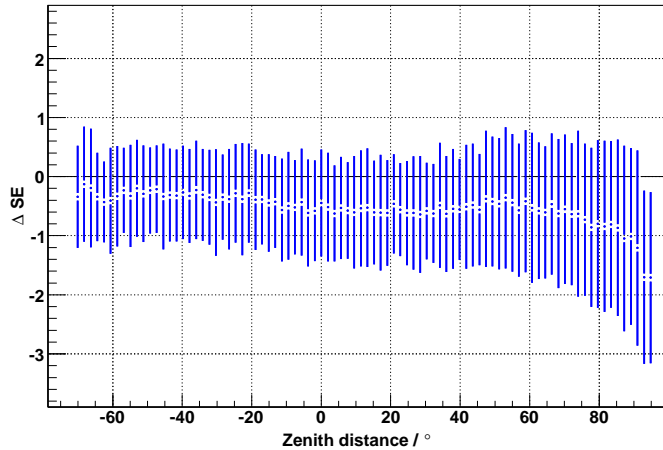


Figure 3: The measured difference between the two shaft-encoders fixed on either side of the elevation axis versus zenith angle. Negative zenith angles mean that the telescope has been flipped over the zenith position to the opposite side. The average offset from zero corresponds to a the twist of the two shaft encoders with respect to each other. The error bars denote the spread of several measurements. Under normal conditions the torsion between both ends of the axis is less than the shaft-encoder resolution.

- The analog transmission of the master’s command torque to the slave is replaced by a direct digital communication (EcoX) of the DKCs. This allows for more robust and precise slave control. Furthermore the motors could be coupled with relative angular synchronism allowing to suppress deformations of the structure by keeping the axis connecting both motors stable.
- A single professional programmable logic controller (PLC), in German: *Speicherprogrammierbare Steuerung* (SPS, type designation Rexroth Bosch, IndraControl SPS L 20) replaces the two MACSs. Connection between the SPS and the DKCs is now realized through a digital Profibus DP interface substituting the analog signals.

- The connection from the SPS to the control PC is realized via Ethernet connection. Since Ethernet is more commonly in use than CANbus, soft- and hardware support is much easier.

#### 4.4. PC control

The drive system is controlled by a standard PC running a Linux operating system, a custom-designed software based on ROOT [17] and the positional astronomy library *slalib* [18].

Algorithms specialized for the MAGIC tracking system are imported from the Modular Analysis and Reconstruction Software package (MARS) [19, 20, 21] also used in the data analysis [22, 23].

##### 4.4.1. Positioning

Whenever the telescope has to be positioned, the relative distance to the new position is calculated in telescope coordinates and then converted to motor revolutions. Then, the micro controllers are instructed to move the motors accordingly. Since the motion is controlled by the feedback of the encoders on the motor axes, not on the telescope axes, backlash and other non-deterministic irregularities cannot easily be taken into account. Thus it may happen that the final position is still off by a few shaft-encoder steps, although the motor itself has reached its desired position. In this case, the procedure is repeated up to ten times. After ten unsuccessful iterations, the system would go into error state. In almost all cases the command position is reached after at most two or three iterations.

If a slewing operation is followed by a tracking operation of a celestial target position, tracking is started immediately after the first movement without further iterations. Possible small deviations, normally eliminated by the iteration procedure, are then corrected by the tracking algorithm.

#### 4.4.2. Tracking

To track a given celestial target position (RA/Dec, J 2000.0, FK 5 [24]), astrometric and misalignment corrections have to be taken into account. While astrometric corrections transform the celestial position into local coordinates as seen by an ideal telescope (Alt/Az), misalignment corrections convert them further into the coordinate system specific to the real telescope. In case of MAGIC, this coordinate system is defined by the position feedback system.

The tracking algorithm controls the telescope by applying a command velocity for the revolution of the motors, which is re-calculated every second. It is calculated from the current feedback position and the command position required to point at the target five seconds ahead in time. The timescale of 5 s is a compromise between optimum tracking accuracy and the risk of oscillations in case of a too short timescale.

As a crosscheck, the ideal velocities for the two telescope axes are independently estimated using dedicated astrometric routines of slalib. For security reasons, the allowable deviation between the determined command velocities and the estimated velocities is limited. If an extreme deviation is encountered the command velocity is set to zero, i.e., the movement of the axis is stopped.

#### 4.5. Fast positioning

The observation of GRBs and their afterglows in very-high energy gamma-rays is a key science goal for the MAGIC telescope. Given that alerts from satellite monitors provide GRB positions a few seconds after their outburst via the *Gamma-ray Burst Coordination Network* [25], typical burst durations of 10 s to 100 s [14] demand a fast positioning of the telescope. The current best value for the acceleration has been set to  $11.7 \text{ mrad s}^{-2}$ . It is constrained by the maximum constant force which can be applied by the motors. Consequently, the maximum allowed velocity can be derived from the distance between the end-switch activation and the position at which a possible damage to the telescope structure, e.g. ruptured cables, would happen. From these constraints, the maximum velocity currently in use,  $70.4 \text{ mrad s}^{-1}$ , was determined. Note that, as the emergency stopping distance evolves quadratically with the travel velocity, a possible increase of

the maximum velocity would drastically increase the required braking distance. As safety procedures require, an emergency stop is completely controlled by the DKCs itself with the feedback of the motor encoder, ignoring all other control elements.

Currently, automatic positioning by  $\Delta\varphi = 180^\circ$  in azimuth to the target position is achieved within 45 s. The positioning time in elevation is not critical in the sense that the probability to move a longer path in elevation than in azimuth is negligible. Allowing the telescope drive to make use of the reverse mode, the requirement of reaching any position in the sky within 30 s is well met, as distances in azimuth are substantially shortened. The motor specifications allow for a velocity more than four times higher. In practice, the maximum possible velocity is limited by the acceleration force, at slightly more than twice the current value. The actual limiting factor is the braking distance that allows a safe deceleration without risking any damage to the telescope structure.

With the upgraded MAGIC II drive system, during commissioning in 2008 August, a maximum acceleration and deceleration of  $a_{az} = 30 \text{ mrad s}^{-2}$  and  $a_{zd} = 90 \text{ mrad/s}^{-2}$  and a maximum velocity of  $v_{az} = 290 \text{ mrad s}^{-1}$  and  $v_{zd} = 330 \text{ mrad s}^{-1}$  could be reached. With these values the limits of the motor power are exhausted. This allowed a movement of  $\Delta\varphi = 180^\circ/360^\circ$  in azimuth within 20 s / 33 s.

#### 4.6. Tracking precision

The intrinsic mechanical accuracy of the tracking system is determined by comparing the current command position of the axes with the feedback values from the corresponding shaft encoders. These feedback values represent the actual position of the axes with highest precision whenever they change their feedback values. At these instances, the control deviation is determined, representing the precision with which the telescope axes can be operated. In the case of an ideal mount this would define the tracking accuracy of the telescope.

In figure 5 the control deviation measured for 10.9 h of data taking in the night of 2007 July 22/23 and on the evening of July 23 is shown, expressed as absolute deviation on the sky taking both axes into account. In almost all cases it is well below the resolution of the shaft encoders, and in 80% of the time it

does not exceed  $1/8$  of this value ( $\sim 10''$ ). This means that the accuracy of the motion control, based on the encoder feedback, is much better than  $1'$  on the sky, which is roughly a fifth of the diameter of a pixel in the MAGIC camera ( $6'$ , c.f. [26]).

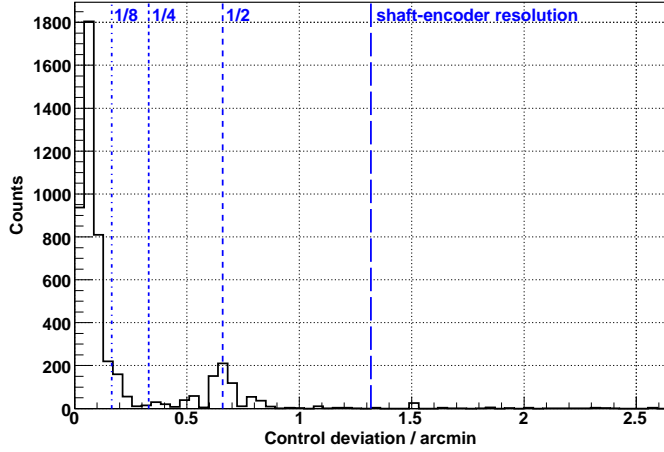


Figure 5: Control deviation between the expected, i.e. calculated, position and the feedback position of the shaft encoders in the moment at which one changes their readout values. For simplicity, the control deviation is shown as absolute control deviation projected on the sky. The blue lines correspond to fractions of the shaft-encoder resolution. The peak at half of the shaft-encoder resolution results from cases in which one of the two averaged elevation encoders is off by one step.

In the case of a real telescope ultimate limits of the tracking precision are given by the precision with which the correct command value is known. Its calibration is discussed hereafter.

## 5. Calibration

To calibrate the position command value, astrometric corrections (converting the celestial target position into the target position of an ideal telescope) and misalignment corrections (converting it further into the target position of a real telescope), have to be taken into account.

### 5.1. Astrometric corrections

The astrometric correction for the pointing and tracking algorithms is based on a library for calculations usually needed in positional astronomy, *slalib* [18]. Key features of this library are the numerical stability of the algorithms and their well-tested

implementation. The astrometric corrections in use (fig. 6) – performed when converting a celestial position into the position as seen from Earth’s center (apparent position) – take into account precession and nutation of the Earth and annual aberration, i.e.,

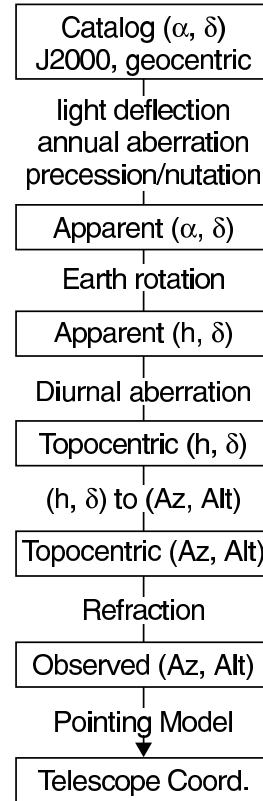


Figure 6: The transformation applied to a given set of catalog source coordinates to real-telescope coordinates. These corrections include all necessary astrometric corrections, as well as the pointing correction to transform from an ideal-telescope frame to the frame of a real telescope.

apparent displacements caused by the finite speed of light combined with the motion of the observer around the Sun during the year. Next, the apparent position is transformed to the observer’s position, taking into account atmospheric refraction, the Earth’s rotation, and diurnal aberration, i.e., the motion of the observer around the Earth’s rotation axis. Some of these effects are so small that they are only relevant for nearby stars and optical astronomy. But as optical observations of such stars are used to *train* the misalignment correction, all these effects are taken into account.

## 5.2. Pointing model

Imperfections and deformations of the mechanical construction lead to deviations from an ideal telescope, including the non-exact alignment of axes, and deformations of the telescope structure.

In the case of the MAGIC telescopes the optical axis of the mirror is defined by an automatic alignment system. This active mirror control is programmed not to change the optical axis once defined, but only controls the optical point spread function of the mirror, i.e., it does not change the center of gravity of the light distribution. This procedure is applied whenever the telescope is observing including any kind of calibration measurement for the drive system. The precision of the axis alignment of the mirrors is better than  $0.2'$  and can therefore be neglected.

Consequently, to assure reliable pointing and tracking accuracy, mainly the mechanical effects have to be taken into account. Therefore the tracking software employs an analytical pointing model based on the TPOINT™ telescope modeling software [27], also used for optical telescopes. This model, called *pointing model*, parameterizes deviations from the ideal telescope. Calibrating the pointing model by mispointing measurements of bright stars, which allows to determine the necessary corrections, is a standard procedure. Once calibrated, the model is applied online. Since an analytical model is used, the source of any deviation can be identified and traced back to components of the telescope mount.

Corrections are parameterized by alt-azimuthal terms [27], i.e., derived from vector transformations within the proper coordinate system. The following possible misalignments are taken into account:

**Zero point corrections (*index errors*)** Trivial offsets between the zero positions of the axes and the zero positions of the shaft encoders.

**Azimuth axis misalignment** The misalignment of the azimuth axis in north-south and east-west direction, respectively. For MAGIC these corrections can be neglected.

**Non-perpendicularity of axes** Deviations from right angles between any two axes in the system, namely (1) non-perpendicularity of

azimuth and elevation axes and (2) non-perpendicularity of elevation and pointing axes. In the case of the MAGIC telescope these corrections are strongly bound to the mirror alignment defined by the active mirror control.

**Non-centricity of axes** The once-per-revolution cyclic errors produced by de-centered axes. This correction is small, and thus difficult to measure, but the most stable correction throughout the years.

## Bending of the telescope structure

- A possible constant offset of the mast bending.
- A zenith angle dependent correction. It describes the camera mast bending, which originates by MAGIC's single thin-mast camera support strengthened by steel cables.
- Elevation hysteresis: This is an offset correction introduced depending on the direction of movement of the elevation axis. It is necessary because the sliding bearing, having a stiff connection with the encoders, has such a high static friction that in case of reversing the direction of the movement, the shaft-encoder will not indicate any movement for a small and stable rotation angle, even though the telescope is rotating. Since this offset is stable, it can easily be corrected after it is fully passed. The passage of the hysteresis is currently corrected offline only.

Since the primary feedback is located on the axis itself, corrections for irregularities of the chain mounting or sprocket wheels are unnecessary. Another class of deformations of the telescope-support frame and the mirrors are non-deterministic and, consequently, pose an ultimate limit of the precision of the pointing.

## 5.3. Determination

To determine the coefficients of a pointing model, calibration data is recorded. It consists of mispointing measurements depending on altitude and azimuth angle. Bright stars are tracked with the telescope at positions uniformly distributed in local coordinates,

i.e., in altitude and azimuth angle. The real pointing position is derived from the position of the reflection of a bright star on a screen in front of the MAGIC camera. The center of the camera is defined by LEDs mounted on an ideal ( $\pm 1$  mm) circle around the camera center, cf. Riegel and Bretz [28].

Having enough of these datasets available, correlating ideal and real pointing position, a fit of the coefficients of the model can be made, minimizing the pointing residual.

### 5.3.1. Hardware and installations

A 0.0003 lux, 1/2" high-sensitivity standard PAL CCD camera (type designation Wattec WAT-902 H) equipped with a zoom lens (type: Computar) is used for the mispointing measurements. The camera is read out at a rate of 25 frames per second using a standard frame-grabber card in a standard PC. The camera has been chosen providing adequate performance and easy readout, due to the use of standard components, for a very cheap price ( $< 500$  Euro). The tradeoff for the high sensitivity of the camera is its high noise level in each single frame recorded. Since there are no rapidly moving objects within the field of view, a high picture quality can be achieved by averaging typically 125 frames (corresponding to 5 s). An example is shown in figure 7. This example also illustrates the high sensitivity of the camera, since both pictures of the telescope structure have been taken with the residual light of less than a half-moon. In the background individual stars can be seen. Depending on the installed optics, stars up to  $12^m$  are visible. With our optics and a safe detection threshold the limiting magnitude is typically slightly above  $9^m$  for direct measurements and on the order of  $5^m \dots 4^m$  for images of stars on the screen.

### 5.3.2. Algorithms

An example of a calibration-star measurement is shown in figure 8. Using the seven LEDs mounted on a circle around the camera center, the position of the camera center is determined. Only the upper half of the area instrumented is visible, since the lower half is covered by the lower lid, holding a special reflecting surface in the center of the camera. The LED positions are evaluated by a simple cluster-finding algorithm looking at pixels more than three standard

deviations above the noise level. The LED position is defined as the center of gravity of its light distribution, its search region by the surrounding black-colored boxes. For simplicity the noise level is determined just by calculating the mean and the root-mean-square within the individual search regions below a fixed threshold dominated by noise.

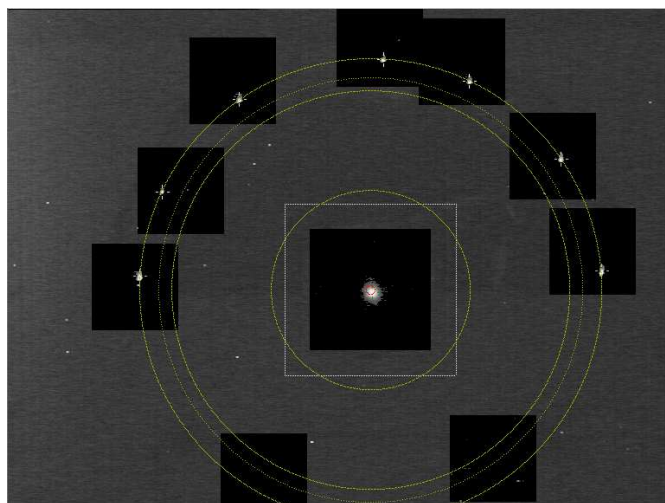


Figure 8: A measurement of a star for the calibration of the pointing model. Visible are the seven LEDs and their determined center of gravity, as well as the reconstructed circle on which the LEDs are located. The LEDs on the bottom part are hidden by the lower lid, holding a screen in front of the camera. The black regions are the search regions for the LEDs and the calibration star. A few dead pixels in the CCD camera can also be recognized.

Since three points are enough to define a circle, from all possible combinations of detected spots, the corresponding circle is calculated. In case of misidentified LEDs, which sometimes occur due to light reflections from the telescope structure, the radius of the circle will deviate from the predefined radius. Thus, any such misidentified circles are discarded. The radius determination can be improved further by applying small offsets of the non-ideal LED positions. The radius distribution is Gaussian and its resolution is  $\sigma \lesssim 1$  mm ( $dr/r \approx 0.3\%$ ) on the camera plane corresponding to  $\sim 1''$ .

The center of the ring is calculated as the average of all circle centers after quality cuts. Its resolution is  $\sim 2''$ . In this setup, the large number of LEDs guarantees operation even in case one LED could not be detected due to damage or scattered light.



Figure 7: A single frame (left) and an average of 125 frames (right) of the same field of view taken with the high sensitivity PAL CCD camera used for calibration of the pointing model. The frames were taken with half moon.

To find the spot of the reflected star itself, the same cluster-finder is used to determine its center of gravity. This gives reliable results even in case of saturation. Only very bright stars, brighter than  $1.0^m$ , are found to saturate the CCD camera asymmetrically.

Using the position of the star, with respect to the camera center, the pointing position corresponding to the camera center is calculated. This position is stored together with the readout from the position feedback system. The difference between the telescope pointing position and the feedback position is described by the pointing model. Investigating the dependence of these differences on zenith and azimuth angle, the correction terms of the pointing model can be determined. Its coefficients are fit minimizing the absolute residuals on the celestial sphere.

#### 5.4. Results

Figure 9 shows the residuals, taken between 2006 October and 2007 July, before and after application of the fit of the pointing model. For convenience, offset corrections are applied to the residuals before correction. Thus, the red curve is a measurement of the alignment quality of the structure, i.e., the pointing accuracy with offset corrections only. By fitting a proper model, the pointing accuracy can be improved to a value below the intrinsic resolution of the system, i.e., below shaft-encoder resolution. In more than 83% of all cases the tracking accuracy is better

than  $1.3'$  and it hardly ever exceeds  $2.5'$ . The few datasets exceeding  $2.5'$  are very likely due to imperfect measurement of the real pointing position of the telescope, i.e., the center of gravity of the star light.

The average absolute correction applied (excluding the index error) is on the order of  $4'$ . Given the size, weight and structure of the telescope this proves a very good alignment and low sagging of the structure. The elevation hysteresis, which is intrinsic to the structure, the non-perpendicularity and non-centricity of the axes are all in the order of  $3'$ , while the azimuth axis misalignment is  $< 0.6'$ . These numbers are well in agreement with the design tolerances of the telescope.

##### 5.4.1. Limitations

The ultimate limit on the achievable pointing precision are effects, which are difficult to correlate or measure, and non-deterministic deformations of the structure or mirrors. For example, the azimuth support consists of a railway rail with some small deformations in height due to the load, resulting in a wavy movement difficult to parameterize. For the wheels on the six bogeys, simple, not precisely machined crane wheels were used, which may amplify horizontal deformations. Other deformations are caused by temperature changes and wind loads which are difficult to control for telescopes without dome, and which cannot be modeled. It should be noted that the

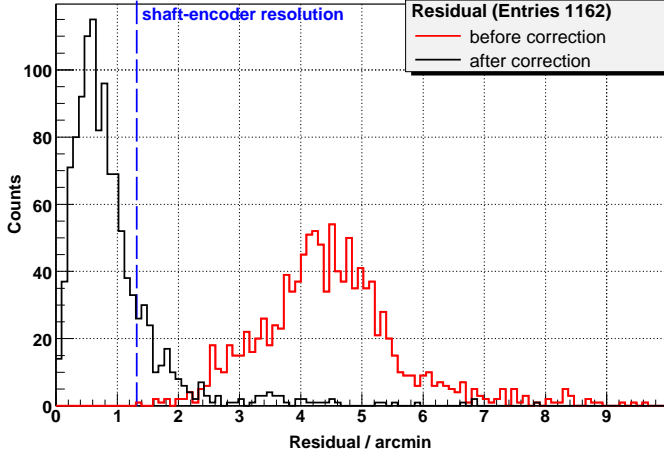


Figure 9: Distribution of absolute pointing residual on the sky between the measured position of calibration stars and their nominal position with only offset correction for both axes (red) and a fitted pointing model (blue) applied. Here in total 1162 measurements were used, homogeneously distributed over the local sky. After application of the pointing model the residuals are well below the shaft-encoder resolution, i.e., the knowledge of the mechanical position of the axes.

azimuth structure can change its diameter by up to 3 cm due to day-night temperature differences, indicating that thermal effects have a non-negligible and non-deterministic influence.

Like every two axis mount, also an alt-azimuth mount has a blind spot near its upward position resulting from misalignments of the axis which are impossible to correct by moving one axis or the other. From the size of the applied correction it can be derived that the blind spot must be on the order of  $\lesssim 6'$  around zenith. Although the MAGIC drive system is powerful enough to keep on track pointing about  $6'$  away from zenith, for safety reasons, i.e., to avoid fast movement under normal observation conditions, the observation limit has been set to  $\theta < 30'$ . Such fast movements are necessary to change the azimuth position from moving the telescope upwards in the East to downwards in the South. In the case of an ideal telescope, pointing at zenith, even an infinitely fast movement would be required.

#### 5.4.2. Stability

With each measurement of a calibration-star also the present pointing uncertainty is recorded. This allows for monitoring of the pointing quality and for offline correction. In figure 10 the evolution of the

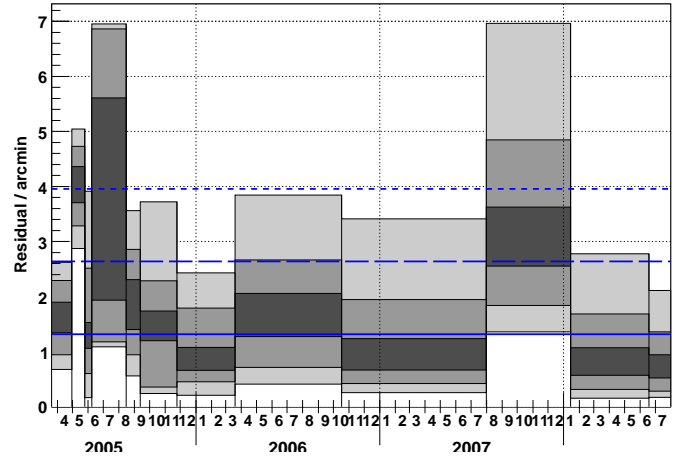


Figure 10: The distribution of mispointing measurements. The measurement is a direct measurement of the pointing accuracy. The plot shows its time-evolution. Details on the bin edges and the available statistics is given in the caption of table 1. Since the distribution is asymmetric, quantiles are shown, from bottom to top, at 5%, 13%, 32%, 68%, 87% and 95%. The dark grey region belong to the region between quantiles 32% and 68%.

measured residuals over the years are shown. The continuous monitoring has been started in March 2005 and is still ongoing. Quantiles are shown since the distribution can be asymmetric depending on how the residuals are distributed on the sky. The points have been grouped, where the grouping reflects data taken under the same conditions (pointing model, mirror alignment, etc.). It should be noted, that the measured residuals depend on zenith and azimuth angle, i.e., the distributions shown are biased due to inhomogeneous distributions on the sky in case of low statistics. Therefore the available statistics is given in table 1.

The mirror focusing can influence the alignment of the optical axis of the telescope, i.e., it can modify the pointing model. Therefore a calibration of the mirror refocusing can worsen the tracking accuracy, later corrected by a new pointing model. Although the automatic mirror control is programmed such that a new calibration should not change the center of gravity of the light distribution, it happened sometimes in the past due to software errors.

The determination of the pointing model also relies on a good statistical basis, because the measured residuals are of a similar magnitude as the accuracy

| Begin      | Counts | Begin      | Counts |
|------------|--------|------------|--------|
| 2005/03/20 | 29     | 2005/11/24 | 38     |
| 2005/04/29 | 43     | 2006/03/19 | 502    |
| 2005/05/25 | 30     | 2006/10/17 | 827    |
| 2005/06/08 | 26     | 2007/07/31 | 87     |
| 2005/08/15 | 160    | 2008/01/14 | 542    |
| 2005/09/12 | 22     | 2008/06/18 | 128    |

Table 1: Available statistics corresponding to the distributions shown in figure 10. Especially in cases of low statistics the shown distribution can be influenced by inhomogeneous distribution of the measurement on the local sky. The dates given correspond to dates for which a change in the pointing accuracy, as for example a change to the optical axis or the application of a new pointing model, is known.

of a single calibration-star measurement. The visible improvements and deterioration are mainly a consequence of new mirror focusing and following implementations of new pointing models. The improvement over the past year is explained by the gain in statistics.

On average the systematic pointing uncertainty was always better than three shaft-encoder steps (corresponding to  $4'$ ), most of the time better than  $2.6'$  and well below one shaft-encoder step, i.e.  $1.3'$ , in the past year. Except changes to the pointing model or the optical axis, as indicated by the bin edges, no degradation or change with time of the pointing model or a worsening of the limit given by the telescope mechanics could be found.

## 6. Scalability

With the aim to reach lower energy thresholds, the next generation of Cherenkov telescopes will also include larger and heavier ones. Therefore more powerful drive systems will be needed. The scalable drive system of the MAGIC telescope is suited to meet this challenge. With its synchronous motors and their master-slave setup, it can easily be extended to larger telescopes at moderate costs, or even scaled down to smaller ones using less powerful components. Consequently, telescopes in future projects, with presumably different sizes, can be driven by similar components resulting in a major simplification of maintenance. With the current setup, a track-

ing accuracy at least of the order of the shaft-encoder resolution is guaranteed. Pointing accuracy – already including all possible pointing corrections – is dominated by dynamic and unpredictable deformations of the mount, e.g., temperature expansion.

## 7. Outlook

Currently, efforts are ongoing to implement the astrometric subroutines as well as the application of the pointing model directly into the Programmable Logic Controller. A first test will be carried out within the DWARF project soon [29]. The direct advantage is that the need for a control PC is omitted. Additionally, with a more direct communication between the algorithms, calculating the nominal position of the telescope mechanics, and the control loop of the drive controller, a real time, and thus more precise, position control can be achieved. As a consequence, the position controller can directly be addressed, even when tracking, and the outermost position control-loop is closed internally in the drive controller. This will ensure an even more accurate and stable motion. Interferences from external sources, e.g. wind gusts, could be counteracted at the moment of appearance by the control on very short timescales, on the order of milli-seconds. An indirect advantage is that with a proper setup of the control loop parameters, such a control is precise and flexible enough that a cross-communication between the master and the slaves can also be omitted. Since all motors act as their own master, in such a system a broken motor can simply be switched off or mechanically decoupled without influencing the general functionality of the system.

An upgrade of the MAGIC I drive system according to the improvements applied for MAGIC II is ongoing.

## 8. Conclusions

The scientific requirements demand a powerful, yet accurate drive system for the MAGIC telescope. From its hardware installation and software implementation, the installed drive system exceeds its design specifications as given in section 2. At the same

time the system performs reliably and stably, showing no deterioration after five years of routine operation. The mechanical precision of the motor movement is almost ten times better than the readout on the telescope axes. The tracking accuracy is dominated by random deformations and hysteresis effects of the mount, but still negligible compared to the measurement of the position of the telescope axes. The system features integrated tools, like an analytical pointing model. Fast positioning for gamma-ray burst followup is achieved on average within less than 45 seconds, or, if movements *across the zenith* are allowed, 30 seconds. Thus, the drive system makes MAGIC the best suited telescope for observations of these phenomena at very high energies.

For the second phase of the MAGIC project and particularly for the second telescope, the drive system has been further improved. By design, the drive system is easily scalable from its current dimensions to larger and heavier telescope installations as required for future projects. The improved stability is also expected to meet the stability requirements, necessary when operating a larger number of telescopes.

## 9. Acknowledgments

The authors acknowledge the support of the MAGIC collaboration, and thank the IAC for providing excellent working conditions at the Observatorio del Roque de los Muchachos. The MAGIC project is mainly supported by BMBF (Germany), MCI (Spain), INFN (Italy). We thank the construction department of the MPI for Physics, for their help in the design and installation of the drive system as well as Eckart Lorenz, for some important comments concerning this manuscript. R.M.W. acknowledges financial support by the MPG. His research is also supported by the DFG Cluster of Excellence “Origin and Structure of the Universe”.

## References

[1] E. Lorenz, *New Astron. Rev.* 48 (2004) 339.  
 [2] J. Cortina et al. (MAGIC Collab.), in: *Proc. 29th Int. Cosm. Ray Conf.*, Pune, India, August 2005, Vol. 5, 359.  
 [3] F. Goebel (MAGIC Collab.), in: *Proc. 30th Int. Cosm. Ray Conf.*, July 2007, Merida, Mexico, preprint (arXiv:0709.2605)

[4] E. Aliu et al. (MAGIC Collab.), *Science*, 16 October 2008 (10.1126/science.1164718)  
 [5] J. Albert et al. (MAGIC Collab.), *ApJ* 642 (2006) L119.  
 [6] J. Albert et al. (MAGIC Collab.), *ApJ* 667 (2008) L21.  
 [7] J. Albert et al. (MAGIC Collab.), *Science* 320 (2008) 1752.  
 [8] R. S. Somerville, J. R. Primack, and S. M. Faber, *Mon. Not. R. Astr. Soc.* 320 (2001) 504.  
 [9] Kneiske, T. M., 2008, *Chin. J. Astron. Astrophys. Suppl.* 8, 219  
 [10] M. G. Hauser and E. Dwek, *ARA&A* 39 (2001) 249.  
 [11] T. M. Kneiske, T. Bretz, K. Mannheim, and D. H. Hartmann, *A&A* 413 (2004) 807.  
 [12] K. Mannheim, D. Hartmann, and B. Funk, *ApJ* 467 (1996) 532.  
 [13] J. Albert et al. (MAGIC Collab.), *ApJ* 667 (2007) 358.  
 [14] W. S. Paciesas et al., *ApJS* 122 (1999) 465.  
 [15] T. Bretz, D. Dorner, and R. Wagner, in: *Proc. 28th Int. Cosm. Ray Conf.*, August 2003, Tsukuba, Japan, Vol. 5, 2943.  
 [16] T. Bretz, D. Dorner, R. M. Wagner, and B. Riegel, in: *Proc. Towards a network of atmospheric Cherenkov detectors VII*, April 2005, Palaiseau, France.  
 [17] ROOT System Home Page, <http://root.cern.ch>.  
 [18] P. T. Wallace, TPOINT – A Telescope Pointing Analysis System, 2001  
 [19] T. Bretz and R. Wagner, in: *Proc. 28th Int. Cosm. Ray Conf.*, August 2003, Tsukuba, Japan, Vol. 5, 2947.  
 [20] T. Bretz and D. Dorner, in: *Proc. Towards a network of atmospheric Cherenkov detectors VII*, April 2005, Palaiseau, France.  
 [21] T. Bretz and D. Dorner, in: *International Symposium on High Energy Gamma-Ray Astronomy*, July 2008.  
 [22] T. Bretz, in: *Proc. 29th Int. Cosm. Ray Conf.*, Pune, India, August 2005, Vol. 4, 315.  
 [23] D. Dorner and T. Bretz, in: *Proc. Towards a network of atmospheric Cherenkov detectors VII*, April 2005, Palaiseau, France, p. 571–575.  
 [24] W. Fricke, H. Schwan, T. Lederle, et al., *Veröffentlichungen des Astronomischen Rechen-Instituts Heidelberg* 32 (1988) 1.  
 [25] Gamma-ray Burst Coordination Network <http://gcn.gsfc.nasa.gov>.  
 [26] C. Baixeras et al. (MAGIC Coll.), in: *Proc. 29th Int. Cosm. Ray Conf.*, Pune, India, August 2005, Vol. 5, 227.  
 [27] P.T. Wallace, SLALIB – Position Astronomy Library 2.5-3, Programmer’s Manual, 2005, <http://star-www.rl.ac.uk/star/docs/sun67.htm>.  
 [28] B. Riegel, T. Bretz, D. Dorner, and R. M. Wagner, in: *Proc. 29th Int. Cosm. Ray Conf.*, Pune, India, August 2005, Vol. 5, 219.  
 [29] T. Bretz et al., in: *Proc. of Workshop on Blazar Variability across the Electromagnetic Spectrum, PoS (BLAZARS2008)074*, Palaiseau, France.